Rock and Soil Mechanics 2025 46(10): 3267−3279 ISSN 1000−7598
https: //doi.org/10.26599/RSM.2024.94300573 journal homepage: rocksoilmech.whrsm.ac.cn

Rock cracking and evolution mechanism under the action of new type of arc-shaped charge blasting

XU Guo-qing[1], HUANG Gao-xiang[2], WANG Xie-kang[1], LUO Deng-ze[3], LI Hong-tao[1], YAO Qiang[1]

1 State Key Laboratory of Hydraulics and Mountain River Engineering, Sichuan University, Chengdu, Sichuan 610065, China

2 Sichuan Academy of Water Conservancy, Chengdu, Sichuan 610072, China

3 Yalong River Hydropower Development Company, Ltd., Chengdu, Sichuan 610051 China

Abstract: The application of shaped charge blasting in smooth blasting during chamber excavation is investigated. Based on the principle of shaped charge jets, an arc-shaped charge structure is proposed. Numerical modeling of arc-shaped charge blasting (ASCB) is established and compared with cone-shaped charge blasting (CSCB). The findings indicate that ASCB consumes 43.4% less explosive than CSCB, and the efficiency of ASCB in the charge direction surpasses that of CSCB by 25.97%. Upon reaching the blast-hole wall, the shock wave of ASCB is more concentrated than that of CSCB, facilitating the formation of initial cracks in the energy-gathering direction. The pressure exerted by ASCB on the energy-gathering side of the blast-hole wall is 6.26% higher than that of CSCB, whereas the pressure on the non-energy-gathering side is 37.34% lower. The crack length generated by ASCB in the energy-accumulation direction is approximately twice that of CSCB. Consequently, it is concluded that the shaped charge blasting effect of ASCB is superior to that of CSCB. These research outcomes offer a novel approach for directional presplitting blasting.

Keywords: ANSYS/LS-DYNA; shaped charge blasting; numerical simulation; fluid-structure coupling; decoupling charge

1 Introduction

The traditional smooth blasting method presents numerous challenges, including the need for a large number of holes, high drilling accuracy requirements, and compromised surrounding rock quality. When the rock mass contains well-developed joint fissures, the efficiency of smooth blasting is low and the formation of the desired shape is difficult, significantly impacting the construction quality and economy of the project. Consequently, shaped charge blasting has been increasingly adopted for smooth blasting. However, there is currently no uniform standard for the configuration of shaped charge blasting, and it cannot be applied in areas with stringent requirements for blasting vibration. Therefore, it is imperative to explore a blasting method that employs less explosive, minimizes damage to the surrounding rock, and reduces the impact on residents and buildings in the vicinity of the construction site.

At present, there are two main types of shaped charge pipe to achieve shaped blasting. The first type is to achieve shaped blasting by cutting the charge pipe in the presplitting direction, which does not cut the explosive[1-3]. At present, there are many related pieces of research, for example, the model test of dynamic fracture effect of blasting crack of slotted tube charge by using digital laser dynamic caustics method[4-6]. Li et al.[7] used the strain gauge method to study the dynamic fracture process of mode I crack in rock directional fracture blasting and compared the calculated results with the results of the dynamic caustics method. The results show that the strain gauge method can approximately record the whole process of rock crack growth, which provides an experimental basis for studying the directional fracture process of opaque materials. The stress and damage evolution process of the blast-hole wall and the structural deformation of the surrounding rock under the slotted tube-shaped charge presplitting blasting can also be obtained through theoretical analysis and numerical simulation[8]. Zhang et al.[9] proposed a new method combining slotted tube-shaped charge blasting with hydraulic blasting and found that shaped charge hydraulic blasting has greater power and higher fracture rate. The energy-gathering effect of this method depends on the strength of energy-gathering tube. If the strength of energy-gathering tube is not enough, a good energy-gathering effect will not be achieved. In addition, this method cannot reduce the number of explosives and the blasting vibration. The second type is to cut a conical groove from the charge in the direction of energy-accumulation and use the characteristics of detonation products moving along the direction of the outer normal of the explosive surface to form a jet at the conical groove[10-14]. The shaped jet is more conducive to the formation of initial cracks, and the charge is smaller after the charge is cut, which is conducive to reducing blasting vibration. The initial cracks in the direction of shaped jet are conducive to

Received: 17 October 2024 Accepted: 8 May 2025
This work was supported by the National Key Research and Development Program of China (2023YFC3008300, 2023YFC3008305), the Sichuan Provincial International Science and Technology Collaboration & Innovation Project (2025YFHZ0165), the National Natural Science Foundation of China (51809188) and the Joint Funds of National Natural Science Foundation of China (U2340201).
First author: XU Guo-qing, male, born in 1997, PhD candidate, focusing on rock dynamics and engineering blasting research. E-mail: 1179913581@qq.com
Corresponding author: YAO Qiang, male, born in 1987, PhD, associate professor, focusing on water conservancy and hydropower project construction and debris flow geological disaster research. E-mail: yaoqiang777@126.com

the penetration of cracks between blast-holes[15]. Pan et al.[16] studied the damage characteristics of soil and concrete caused by conventional blasting and cone-shaped charge blasting (CSCB) through model tests and quantitatively analyzed the blasting damage law and energy distribution. CSCB can also be combined with hydraulic blasting to improve the efficiency of rock breaking[17].

The directional presplitting blasting of slotted pipes depends on the strength of slotted pipes, and steel pipes are mostly used as charging pipes. However, steel pipes are rarely used in smooth blasting, which is expensive and inconvenient to load explosives, so it is difficult to promote their application. CSCB uses PVC pipe as the energy-gathering device, which can reduce blasting vibration and damage to the surrounding rock. However, it can be seen from its energy-gathering principle that some of the energy in the energy-gathering direction counteracts each other, and the energy is concentrated in a certain area of the blast-hole wall, rather than at a point on the blast-hole wall, so the role of energy concentration cannot be fully played. To overcome the disadvantages of the slotted tube-shaped charge blasting and CSCB, arc-shaped charge blasting (ASCB) was proposed. Through numerical simulation, the effect of ASCB is compared with that of the CSCB, hoping to improve the application of shaped charge blasting in practical projects.

2 Mechanism analysis of ASCB

2.1 The mechanism of shaped charge blasting between ASCB and CSCB

In the process of shaped charge blasting, the shaped charge jet first reaches the blast-hole wall, and the velocity and energy of the shaped charge jet are both greater than the velocity and energy of the detonation products in the non-shaped charge direction, resulting in the rock in the shaped charge direction of the blast-hole wall being crushed to form an initial crack, and the temperature in the blast-hole rising sharply. As the shock wave propagates outward, the strength of the shock wave also decreases rapidly until the pressure generated by the shock wave is less than the dynamic compressive strength of the rock, at which time the crushing zone stops expanding. Subsequently, the shock wave attenuates into a stress wave in the rock mass and generates tangential tensile stress. When the tangential tensile stress is greater than the dynamic tensile strength of rock, the rock mass will produce radial cracks. Finally, the radial crack further propagates under the quasi-static pressure of stress wave and detonation gas[18-19]. Since the initial crack is generated first in the direction of energy-accumulation, the crack tip in the direction of energy-accumulation will produce a strong stress concentration, and finally, the main crack will be formed in the direction of energy-accumulation, and the secondary crack will be formed in the direction of non-energy-accumulation[20].

The difference in the energy-accumulation effect between CSCB and ASCB is mainly determined by the initial crack. After the initial crack is generated, stress concentration will be formed at the crack tip, which will promote the further expansion of the crack. Therefore, the direction and position of the initial crack on the blast-hole wall affect the final shape of the crack area[21-22]. As shown in Fig.1, after the conical slot jet is shot along the normal direction outside the cone surface, some of the jets cancel each other, thus losing part of the energy. As a result, the energy is not concentrated at one point on the blast-hole wall, but is dispersed in a certain area. Therefore, the initial cracks are generated in this area at the same time, reducing the energy-accumulation effect. CSCB cannot avoid this defect no matter how to adjust the decoupling coefficient and the angle of the tapered groove, while ASCB can avoid this problem very well.

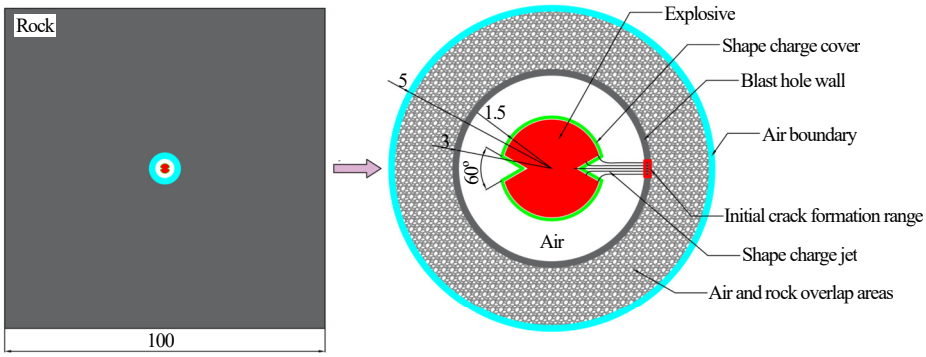


Fig.1 Numerical models of CSCB (unit: cm)

The jet generated by ASCB is shown in Fig.2. After the jet is shot along the normal direction outside the arc surface, it is concentrated at a point on the blast-hole wall. Therefore, the initial crack is only generated in a small area near this point, thus avoiding the dispersion of the jet and enhancing the effect of energy-accumulation. ASCB can adapt to charges and blast-holes of different diameters, as shown in Fig.3(a). For a variety of uncoupled charge structures, it is only necessary to control the center of the arc surface to be at the energy-gathering point of the blast-hole wall, and satisfy:

$$R-r<R_0<R \tag{1}$$

where R_0 is the radius of the cutting arc; r is the radius of the explosive; R is the radius of the blast-hole. A reasonable range for R_0 is as follows:

$$R_0 = R - \frac{r}{k} \tag{2}$$

where k is a charge cutting parameter.

The variation of peak pressure at characteristic points on the borehole wall in the direction of energy concentration and non-energy concentration with the change of k was investigated through numerical simulation. The results are shown in Fig.3(b), where k=0 represents a circular cross-section of the charge column without cutting, and the peak pressure is isotropic at this time. As the k increases, the cut part of the charge column increases and the amount of explosive decreases, hence the peak pressure on the borehole wall in both the energy concentration and non-energy concentration directions gradually decreases. However, the non-energy concentration direction shows a less significant decrease after the k reaches 1.5. Therefore, to ensure a lower peak pressure in the non-energy concentration direction while maintaining a higher level in the energy concentration direction, it is recommended that the reasonable range for k be controlled between 1.5 and 3.0.

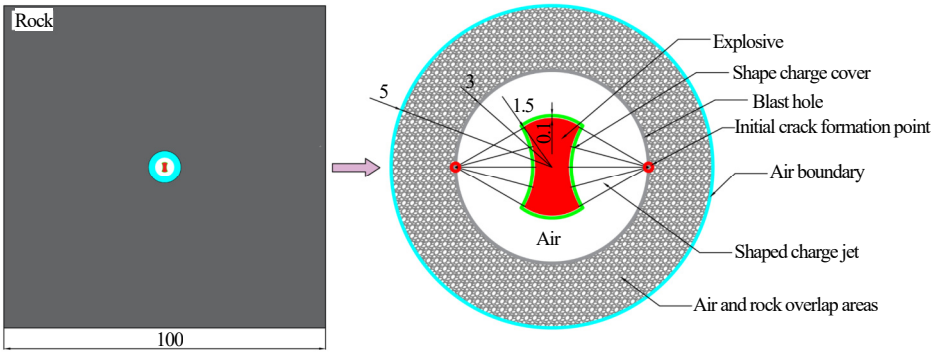
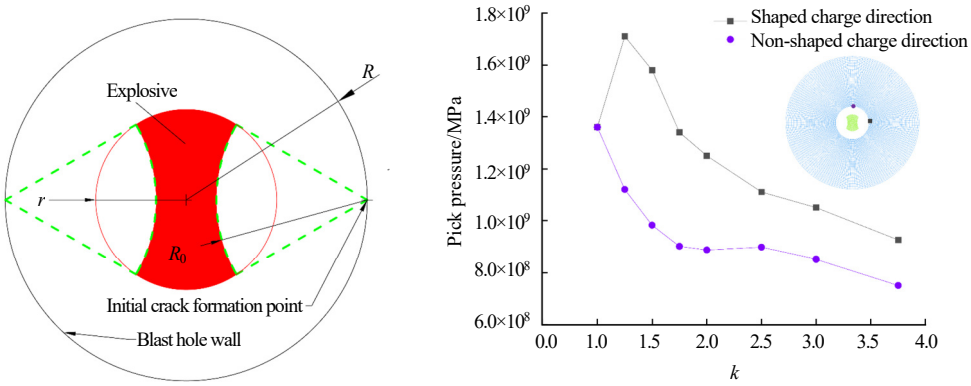


Fig.2 Numerical models of ASCB (unit: cm)



(a) Explosives cross-section of ASCB (b) Peak pressure variation on borehole wall with k

Fig.3 Section cutting control parameters of ASCB

2.2 Effective charge analysis of ASCB and CSCB

When the explosive is surrounded by multiple planes, the detonation products also scatter outward from the normal direction of these planes, and these parts are the effective parts in that direction. The damage suffered by the target object facing its effective part near the charge is the impact effect of the effective part detonation product. The ratio of the volume of the effective part of the detonation product to the volume of the overall charge is defined as the charge utilization rate[23].

For CSCB, based on the analysis results of Li[23] and considering the symmetry of the explosive cross-section, the first quadrant was selected as the research object, as shown in Fig.4. Curve *IG* represents the boundary of shaped charge detonation products. The detonation products below curve *IG* scatter outward from *GE*, while the detonation products above curve *IG* scatter outward from *AG*. *C* is the point on the curve *IG*, the shortest distance between this point and arc *AG* is *CB*, and the shortest distance between this point and straight line *EG* is *CD*. By making *CB* equal to *CD*, the implicit function equation of the *IG* curve can be obtained, and then the cubic polynomial fitting of this equation can be performed by the least square method. The expression for the efficiency of charge in the direction of energy accumulation is as follows:

$$\eta = \frac{S_1 - S_2}{S_2 - S_3} \times 100\% \tag{3}$$

where S_1 is the area of polygon *IGHO*; S_2 is the area of polygon *AGHO*; and S_3 is the area of polygon *GHE*.

In this study, the section radius of CSCB is *OA*=1.5 cm, the distance between the cone apex and the center is

OE=0.7 cm, and the half cone angle is α=30°, then the expression of curve IG is y=0.059 $9x^3$−0.350 $2x^2$+0.245 $9x$+0.618. Obtained through integration: S_1=0.858 7 cm^2，S_2=1.748 3 cm^2，S_3=0.156 1 cm^2, the area of charge is S=1.592 2 cm^2. The effective efficiency of charge in the direction of energy accumulation η=44.13%.

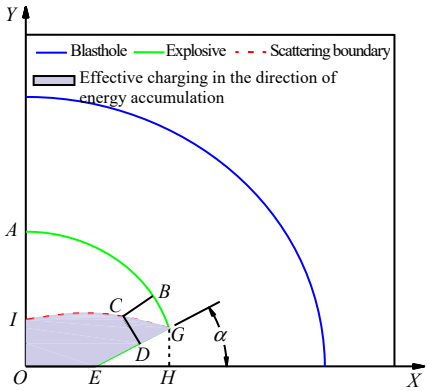


Fig.4 Effective charge analysis model for CSCB

For ASCB, a grain explosion analysis model can be established as shown in Fig.5. The analytical formula for the function of arc AG in the first quadrant is

$$y=\sqrt{a^2-x^2} \tag{4}$$

The analytical formula for the function of arc GE in the first quadrant is

$$y=\sqrt{b^2-(x-c)^2} \tag{5}$$

where arc AG is an arc with O as the center and AO as the radius, and its radius is set to a; arc GE is an arc with F as the center and EF as the radius, and its radius is set to b. A blast hole is a circle with O as the center and OF as the radius, and its radius is set to c.

According to the above equation, the intersection coordinates $G(m, n)$ of arc AG and arc GE can be solved, and it can be obtained that:

$$\left.\begin{aligned} m&=\frac{a^2+c^2-b^2}{2c}\\ n&=\frac{\sqrt{2a^2c^2+2b^2c^2+2a^2b^2-a^4-c^4-b^4}}{2c}\end{aligned}\right\} \tag{6}$$

Assuming $C(x_0, y_0)$ is the point on the boundary of the effective part of the charge in the direction of charge formation, according to the instantaneous detonation assumption, the distance $|CB|$ from this point to the arc AG is equal to the distance $|CD|$ to the arc GE. Among them:

$$\left.\begin{aligned} |CB|&=a-\sqrt{x_0^2+y_0^2}\\ |CD|&=\sqrt{(x_0-c)^2+y_0^2}-b\end{aligned}\right\} \tag{7}$$

Make $|CB|$ equal to $|CD|$, the boundary functional equation can be obtained as follows:

$$\sqrt{x_0^2+y_0^2}+\sqrt{(x_0-c)^2+y_0^2}=a+b \tag{8}$$

The above equation is an Implicit function equation, which is difficult to solve. The coordinates of 100 points within x in (0, m) of the implicit function can be obtained uniformly through Python, and the obtained points are fitted with a third-order polynomial by the least square method. Make the independent variable is X, and the dependent variable is Y, then the polynomial function expression can be obtained as follows:

$$Y=\beta_3X^3+\beta_2X^2+\beta_1X+e \tag{9}$$

The effective efficiency of charge in the direction of energy accumulation is:

$$\eta=\frac{S_1-S_3}{S_2-S_3}\times100\% \tag{10}$$

$$\left.\begin{aligned} S_1&=\int_0^m(\beta_3X^3+\beta_2X^2+\beta_1X)\mathrm{d}x=\frac{1}{4}\beta_3m^4+\frac{1}{4}\beta_2m^3+\frac{1}{4}\beta_1m^2+em\\ S_2&=\int_0^m\sqrt{a^2-x^2}\,\mathrm{d}x=\frac{a^2}{2}\arcsin\frac{m}{a}+\frac{m}{2}\sqrt{a^2-m^2}\\ S_3&=\int_{c-b}^m\sqrt{b^2-(x-c)^2}\,\mathrm{d}x=\frac{b^2}{2}\left(\arcsin\frac{m-c}{a}+\arcsin\frac{b}{a}\right)+\frac{m-c}{2}\sqrt{b^2-(m-c)^2}\end{aligned}\right\} \tag{11}$$

In this study, the cross-sectional radius of ASCB is $a=1.5$ cm, the length of EF is $b=2.5$ cm, and the radius of the blast hole is $c=3.0$ cm. Therefore, the expression for the curve IG is y =0.117 $5x^3$−0.437 $6x^2$+0.729 $2x$+0.875 8. By integrating, it can be inferred that: S_1=0.912 8 cm^2, S_2=1.182 3 cm^2, S_3=0.281 1 cm^2, the charge area is S=0.901 2 cm^2, and the effective rate of charge in the direction of energy accumulation η=70.10%.

Consequently, it can be concluded that in the numerical simulation of this study, the charge amount of the ASCB is reduced by 43.4% compared to the CSCB. The effective charging area of ASCB in the charging direction is 0.631 7 cm^2, while the effective charging area of CSCB in the charging direction is 0.702 6 cm^2. The effective rate of ASCB in the charge direction is 25.97% higher than that of CSCB in the charge direction.

3 Creation of ASCB and CSCB numerical models

In this study, the numerical model of shaped charge blasting is established by using ANSYS/LS-DANA. ANSYS/LS-DYNA is widely used in shock dynamics involving large deformation nonlinear material properties and multi object contact problems, and can effectively simulate the propagation process of the stress wave and blasting damage in blasting numerical simulation[24-29].

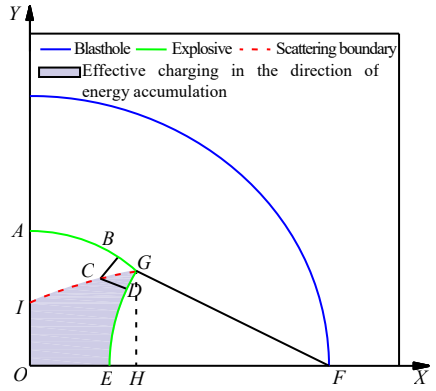


Fig.5 Effective charge analysis model for ASCB

The large deformation caused by explosion shock waves often leads to negative volume in the finite element model, so the fluid-solid coupling method of multi-material is adopted in this study. The arbitrary Lagrangian-Eulerian (ALE) algorithm is used for explosives, PVC-shaped tubes, and air, and the Lagrange algorithm is used for the rock[30]. The inner boundary of the air area and the outer boundary of the explosive area share the same node, and the air area and the rock area partially overlap to transfer the detonation energy. The non-reflective boundary condition is used to make the stress wave propagate infinitely in the rock mass. Since the detonation pressure is far greater than gravity, the effect of gravity is not considered in this study. The total time of simulation is 360 μs. The time is determined by numerical simulation, which can ensure the full expansion of the crack. The unit system used in the numerical simulation is kg-m-s.

To save calculation time, half of the model is established considering the symmetry of the structure. In ASCB, the explosive radius is 0.015 m, the arc radius is 0.025 m, the blast-hole radius is 0.03 m, the thickness of the shaped charge tube is 0.001 m, the diameter of the air area is 0.1 m, and the length and width of the simulated rock area are both 1 m, as shown in Fig.2. Compared with ASCB, only the shapes of explosives and shaped charge tubes of CSCB are different, and the cone angle of the shaped charge groove is 60°, as shown in Fig.1. The thickness of all models is 0.01 m.

In this study, the rock material models were constructed utilizing the plastic-kinematic hardening model. This model incorporates strain rate effects, with the Cowper-Symonds model employed to account for the influence of strain rate on material strength. Crack propagation and rock mass failure are simulated using MAT-ADD-EROSION, with rock elements being removed upon reaching the set value for any of the tensile stress, compressive stress, or shear strain indicators[31-33]. All of the material parameters are shown in Table 1−4[30].

The material model used for explosives is *MAT_HIGH_EXPLOSIVE_BURN. Parameters that need to be entered into this model include explosive density ρ_0, detonation velocity D and blast pressure PCJ. The pressure, energy, and volume expansion characteristics of detonation products generated during explosive explosion are described by the JWL (Jones-Wilkins-Lee) equation. The pressure generated by the explosive explosion is:

$$P = A(1-\frac{\omega}{R_1V})\mathrm{e}^{-R_1V} + B(1-\frac{\omega}{R_2V})^{-R_2V} + \frac{\omega E_0}{V} \quad (12)$$

where P is the pressure applied to the blast-hole wall by a unit detonation product; V is the relative volume of the detonation product; E_0 is the initial internal energy density of the detonation product; and A, B, R_1, R_2 and ω are material constants determined by blasting experiments[33].

The material model of the PVC-shaped charge pipe is *MAT_JOHNSON_COOK. This material model can simulate the conversion process of a PVC-shaped charge tube from solid to gas at ultra-high explosion temperature. In the simulation, since the contribution of PVC-shaped charge tube to detonation products after gasification is very small, the role of its gas products is ignored, and its role in the equation of state is only to ensure smooth calculation. The effective yield stress is:

$$\sigma_y = (A_0 + B_0\bar{\varepsilon}^{\mathrm{p}^n})(1 + C_0 \ln \dot{\varepsilon}^*)(1 - T^{*m}) \quad (13)$$

where A_0, B_0, C_0, n and m are the material physical property constants; σ_y is the effective yield stress; $\dot{\varepsilon}^*$ is the normalized effective plastic strain rate, $\bar{\varepsilon}^{\mathrm{p}^n}$ is the effective plastic strain; and T^* is the temperature at the time of melting.

The material model of air is *MAT_NULL, and the equation of state is *EOS_LINEAR_POLYNOMIAL. The pressure of air is:

$$P = C_0 + C_1\mu + C_2\mu^2 + C_3\mu^3 + (C_4 + C_5\mu + C_6\mu^2)E \quad (14)$$

$$\mu = \frac{1}{V_0} - 1 \quad (15)$$

where C_1, C_2, C_3, C_4, C_5 and C_6 are the coefficients of the equation of state; V_0 is the initial relative volume; and E is the initial internal energy per unit volume.

Table 1 Parameters of explosive

ρ_0/(kg • m^{-3})	D/(m • s^{-1})	PCJ/Pa	A/Pa	B/Pa	R_1	R_2	E_0/Pa	ω	V_0
1.27×10^3	4.2×10^3	7.4×10^9	2.144×10^{11}	1.8×10^8	4.15	0.95	4.19×10^9	0.15	1

Table 2 Parameters of PVC material

Density /(kg • m^{-3})	Specific heat capacity/(J •kg^{-1} •K^{-1})	Melt temperature/K	Room temperature/K	Tensile failure stress /Pa
1.24×10^3	1.18×10^3	368.15	298.15	−261.6

Table 3 Parameters of air

ρ_0(kg • m^{-3})	C_{1-4}	C_5	C_6	E_0/Pa	V_0
1.25	0	0.4	0.4	2.5×10^5	1

Table 4 Parameters of rock

Density /(kg • m^{-3})	Modulus of elasticity /Pa	Poisson's ratio	Yield strength /Pa	Shear modulus /Pa	Minimum hydrostatic pressure /Pa	Maximum hydrostatic pressure /Pa	Effective plastic strain
2.1×10^3	1.5×10^{10}	0.34	1.9×10^7	1×10^9	-3×10^6	3×10^7	0.04

4 Numerical simulation results and analysis

4.1 Propagation of the initial shock wave

The initial shock wave propagation process of the CSCB is shown in Fig.6. At t=3.6 μs, the explosive package is completely detonated. At t=7.2 μs, a shaped jet appears in the direction of energy-gathering. At t=10.8 μs, the shaped jet first reaches the blast-hole wall, and the strength of the shock wave exceeds the compressive strength of the rock and forms an initial crack. At t=14.4 μs and t=18.0 μs, the shock wave has an obvious concentration in the direction of energy-accumulation, and the pressure in the blast-hole exceeds the compressive strength of the rock mass, which causes the rock on the blast-hole wall to be crushed. At t=18.0 μs, the shock wave in the direction of energy-gathering reaches the air boundary faster, and the shock wave in the direction of non-energy-gathering distributes uniformly. At t=25.2 μs, the shock wave in the non-energy-gathering direction reaches the air boundary, and there are many cracks in the non-energy-gathering direction, but only one crack is produced in the energy-gathering direction.

The initial shock wave propagation process of ASCB is shown in Fig.7, when t=3.6 μs, the explosive package is completely detonated. At t=7.2 μs, the intensity of the shock wave is higher in the non-energy-gathering direction because of more charges. At t= 10.8 μs, because of the existence of the arc-shaped trough, an obvious energy concentration phenomenon appears in this direction. At this time, the shock wave reaches the blast-hole wall, causing the blast-hole wall to be crushed. At t=14.4 μs to t=21.6 μs, the shock wave has an obvious concentration in the direction of energy-accumulation, and weakens obviously of non-energy-accumulation. At t= 25.2 μs, the damage of the blast-hole wall in the energy-gathering direction is in the direction greater than that in the non-energy-gathering direction. The strength of the shock wave in the energy-gathering direction is still greater than the compressive strength of rock. The strength of the shock wave in the non-energy-gathering direction can

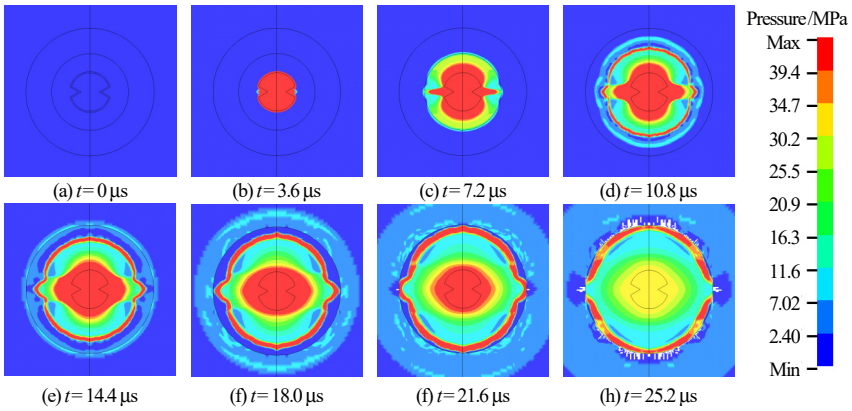


Fig.6 Initial shock wave propagation process of CSCB

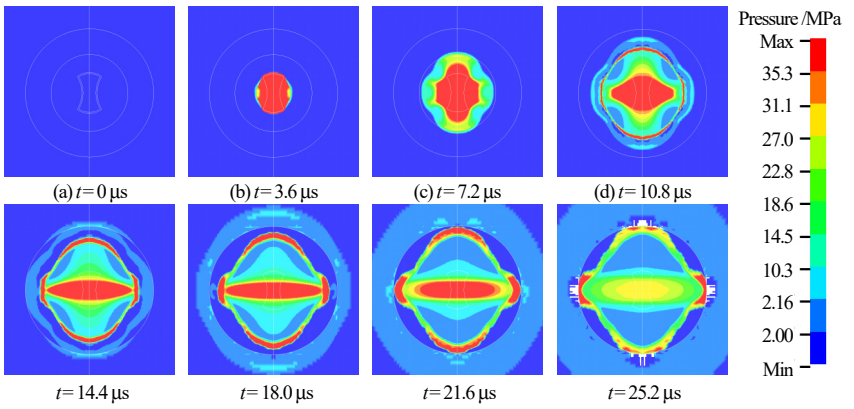


Fig.7 Initial shock wave propagation process of ASCB

no longer cause compression damage to the blast-hole wall, and the shock wave in the 45°, 135°, 225° and 315° directions has obvious hysteresis.

Comparing the propagation process of the initial stress wave of CSCB with that of the initial shock wave of ASCB, it can be found that the overall energy of CSCB exceeds that of ASCB due to the larger charge of CSCB. From the results of energy concentration and initial crack development, it can be concluded that ASCB is more effective and more conducive to forming narrow initial cracks and reducing energy loss in the non-energy-gathering direction.

4.2 Time-history curve of blast-hole wall pressure

To obtain the pressure time history curve of the blast-hole wall, the keyword of control unit failure is deleted, and the characteristic unit is selected in the energy-gathering direction and non-energy-gathering direction of the blast-hole wall to derive the pressure time history curve of these two units. The distribution of peak pressure on the borehole wall is shown in Fig.8. It can be seen that the impact pressure generated by ASCB and CSCB in the transverse direction is significantly higher than that in the longitudinal direction. The impact pressure generated by ASCB in the longitudinal direction is smaller than that of CSCB, while the impact pressure in the transverse direction is similar to the latter.

The time-history curve of blast-hole wall pressure is shown in Fig.9. For CSCB, the peak pressure in the non-energy-gathering direction is 0.324 GPa, and the time is t=14.4 μs. The peak pressure in the direction of energy-accumulation is 0.878 GPa, and the time is t=10.8 μs. Therefore, the pressure peak in the direction of energy-accumulation occurs earlier. For ASCB, the peak pressure in the non-concentrated direction is 0.203 GPa, and the time is t=10.8 μs. The peak pressure in the direction of energy-accumulation is 0.933 GPa, and the time is t= 14.4 μs. The pressure peak in the non-concentrated direction appears earlier. The time when the pressure peak occurs is controlled by two factors: the shaped charge effect and the charge shape. For CSCB, the influence of the tapered groove on the reduction of the charge in the energy-accumulation direction is lower than the shaped charge effect, so the pressure peak appears first in the energy-accumulation direction. For ASCB, the overall charge structure is approximately rectangular, and compared to the concentrated energy direction, the non-shaped charge energy direction is closer to the borehole wall. Therefore, the detonation products of the explosive reach the borehole wall faster than the shaped charge direction after detonation. By comparing the results of CSCB and ASCB, it can be seen that the peak pressure of ASCB is 6.26% higher than that of CSCB in the energy-accumulation direction of the blast-hole wall, indicating that ASCB is more conducive to the generation of initial fractures in the energy-accumulation direction than CSCB. In the non-concentrated direction of the blast-hole wall, the peak pressure of ASCB is 37.34% less than that of CSCB, which can reduce the damage to the blast-hole wall in the non-concentrated direction.

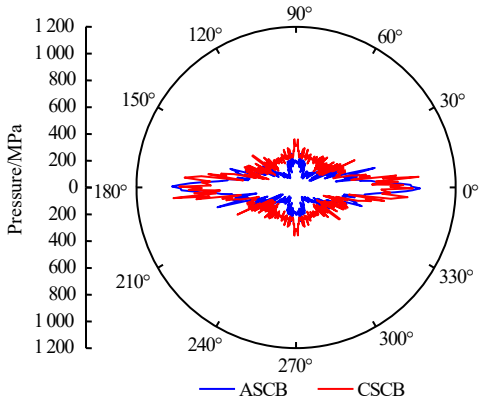


Fig.8 Distribution of peak pressure on the borehole wall

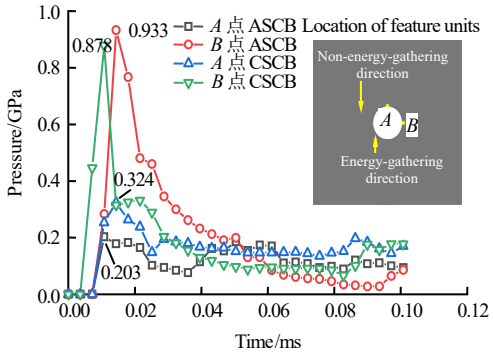


Fig.9 Pressure time history curves of feature units of the borehole wall

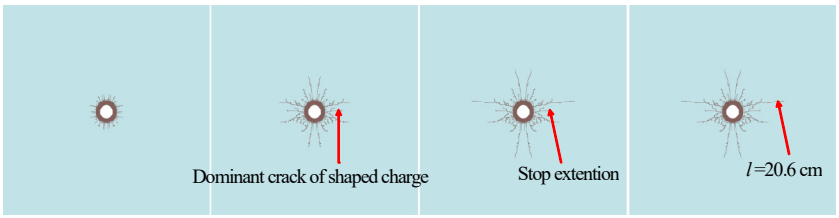
4.3 Crack growth of rock mass

The crack growth of the rock mass of CSCB is shown in Fig.10. At t =32 μs, the crushing zone has been completely formed, and the fracture zone starts to expand outward, at this time, the fractures are not concentrated in the direction of energy-accumulation. At t =104 μs, the crack continues to expand, and a crack appears in the direction of energy-accumulation, but the length of this crack is significantly shorter than its adjacent two cracks. At t =216 μs, the cracks in the direction of energy-accumulation do not continue to expand, and longer cracks appear in the direction of non-energy-accumulation. From t= 216 μs to t=360 μs, all of the cracks stop expanding, and finally, the longest crack appears in the non-energy-concentration direction, and the linear length from the start to the end of the crack (l) is about 20.6 cm.

The rock crack propagation of ASCB is shown in Fig.11. At t=32 μs, the crushing zone continues to expand, and the crushing zone in the direction of energy-concentration is larger than that in the direction of non-energy-accumulation, which is consistent with the lag result of the stress wave in the direction of non-energy-accumulation, and there are cracks in the direction of energy-accumulation. At t=104 μs, the fracture zone gradually expands, and there are dominant fractures in the energy-accumulation direction, and the number and length of fractures in the energy-accumulation direction are more and longer than those in the

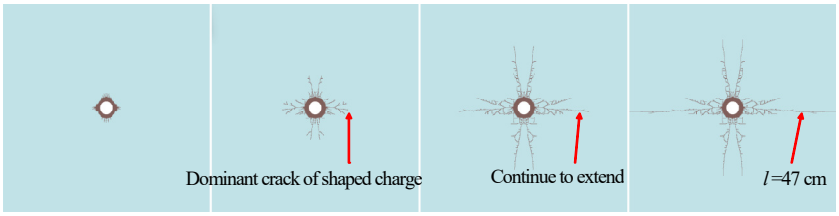
non-energy-accumulation direction. At t =216 μs, the dominant fractures continue to expand, and the dominant fractures in the direction of energy-accumulation expand faster. At t =360 μs, the dominant fracture completely penetrates the rock mass boundary, and the linear length from the starting point to the end point of the dominant fracture is about 47.0 cm.

By comparing the failure process of CSCB and ASCB, it can be found that the dominant cracks in ASCB can continue to expand, and explosive gas in ASCB acts for a longer time, thus eventually forming through-going cracks. However, because the energy of CSCB cannot be concentrated in a small range, resulting in energy dispersion, it cannot achieve a good energy-accumulation effect.



(a) t=32 μs (b) t=104 μs (c) t=216 μs (d) t=360 μs

Fig.10 Rock mass failure process of CSCB



(a) t=32 μs (b) t=104 μs (c) t=216 μs (d) t=360 μs

Fig.11 Rock mass failure process of ASCB

4.4 Physical experimental verification

To verify the numerical results, we conducted a series of polymethyl methacrylate (PMMA) blasting model experiments. PMMA, like rock, is a brittle material and is widely used as a simulant for rock blasting model tests due to its good machinability, isotropy, and homogeneity[34-35]. The dimensions of PMMA plate were 800 mm× 800 mm× 10 mm, with a 40 mm diameter boreholwe centered in the plate. To fully utilize the quasi-static effect of the explosive gas, two steel plates measuring 900 mm×900 mm×6 mm were fixed with eight bolts, sandwiching the PMMA plate. Additionally, to prevent stress concentration from local deformation, a 1 mm thick rubber sheet was placed between the steel plates and the PMMA plate, as shown in Fig.12. In the experiments, 2# rock emulsion explosive with a density of approximately 1.15 g/cm³ and a detonation velocity of about 4 800 m/s was initiated using digital electronic detonators. To minimize the impact of the detonator shock wave on the PMMA plate, the detonator only contacted the explosive without being embedded in it. The charge amount for the CSCB emulsion explosive was 3.41 g, and for the ASCB, it was 2.47 g. Limited by the size of the PMMA plate and to enhance the directional crack formation of the shaped charge blasting, the energy direction was set along the diagonal of the PMMA plate.

The results are shown in Fig.13, where significant main cracks were observed under both charge structures, however, the crack direction did not coincide with the diagonal. There are two possible reasons for this: First, the placement and adjustment of the shaped charge in the borehole were done by eye, which could have introduced some errors. Second, the cracks produced by the blasting process inherently possess a high degree of randomness, making it difficult for a single borehole blast to direct the crack development entirely along a predetermined path. The results indicated that the main crack length produced by ASCB reached 51.4 cm, forming a through-going crack, while the main crack length caused by CSCB was 35.8 cm, not forming a through-going crack. ASCB produced longer secondary cracks in the non-shaping direction compared to CSCB. The model test results were in good agreement with the numerical simulation results, verifying the reliability of the numerical simulation outcomes.

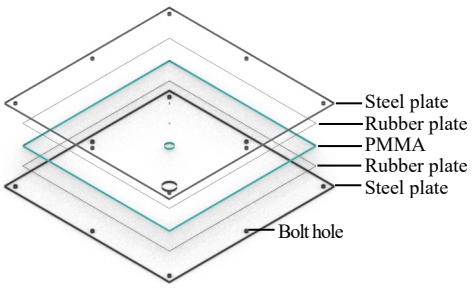
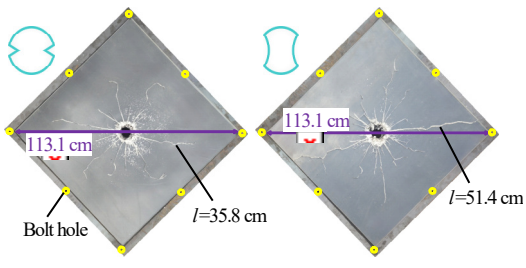


Fig.12 Structure of PMMA blasting model test device



(a) CSCB (b) ASCB

Fig.13 Test result

5 Discussion on the effectiveness of ASCB

To verify the effectiveness of ASCB, ASCB numerical models with different strengths, various uncoupled coefficients, and double-hole blasting were established, and CSCB numerical models were established for comparison. It can be seen from Fig.11 that although through-going cracks have been formed in the energy-gathering direction, the damage to the surrounding rock in the non-energy-gathering direction is also very serious. Considering that in the actual situation, interval charging is often used for smooth blasting, so the movement of detonation products along the direction of the blast hole is not constrained. Therefore, the following finite element model is established without restricting the explosives along the direction of the blast-hole, to reduce the damage to the surrounding rock[36].

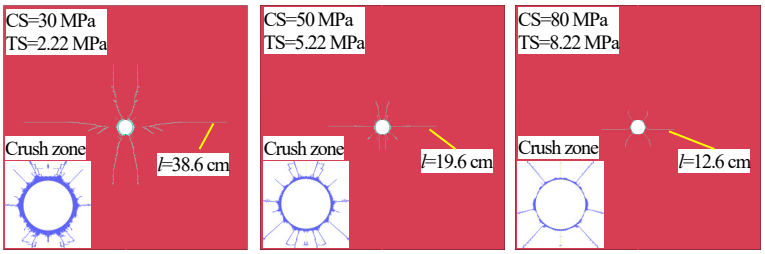
5.1 Shaped charge blasting of rocks with different strengths

Based on compressive strength grade R_b, the strength of rock can be divided into soft rock ($R_b \leqslant 30$ MPa), medium hard rock (30 MPa$<R_b\leqslant$60 MPa) and hard rock ($R_b>$ 60 MPa)[37]. And the tensile strength of rocks is usually 1/25 to 1/4 of the compressive strength. Usually taken as 1/10[38]. By changing the compressive strength and tensile strength of rocks to simulate the shaped charge blasting of rocks with different strengths. Three groups of common rock strength parameters are selected, as shown in Table 5.

Table 5 Rock parameters with different strengths

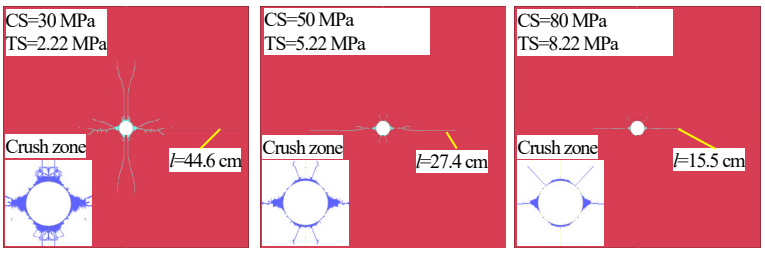
Rock type	Compressive strength/MPa	Tensile strength/MPa
Soft rock	30	2.22
Medium hard rock	50	5.22
Hard rock	80	8.22

In soft rock, medium hard rock and hard rock, the main fracture length of CSCB rock mass is 38.6 cm, 19.6 cm and 12.6 cm, respectively, as shown in Fig.14; the length of main fractures in ASCB rock mass is 44.6 cm, 27.4 cm and 15.5 cm, respectively, as shown in Fig.15. Compared with the length of main fractures formed by CSCB, the length of ASCB main fractures in soft rock, medium hard rock and hard rock increased by 15.5%, 39.8% and 23.0%, respectively. In soft rock, the length of secondary cracks in the non-energy concentration direction of the two kinds of concentrated energy blasting is basically the same, but the cracks formed by ASCB are more concentrated, and the two kinds of concentrated energy blasting modes have serious damage to the rock mass in the non-concentrated direction. In medium hard rock and hard rock, the damage to rock mass in the direction of non-energy-accumulation is significantly reduced, and the number of secondary cracks generated by ASCB is less and the length is shorter than that of CSCB.



(a) Soft rock (b) Medium hard rock (c) Hard rock

Fig.14 Final failure results of CSCB under different rock strengths



(a) Soft rock (b) Medium hard rock (c) Hard rock

Fig.15 Final failure results of ASCB under different rock strengths

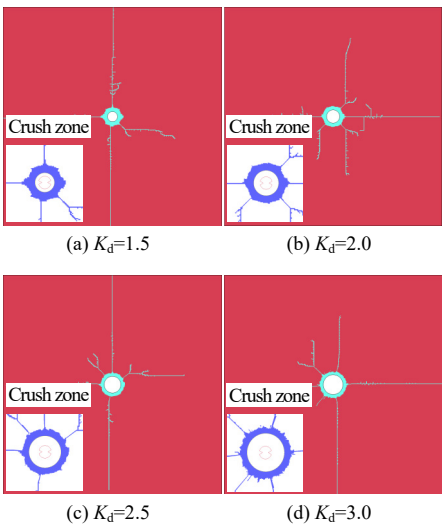
It can also be seen from the figure that the crushing area decreases with the increase in rock strength, the crushing area of CSCB is uniformly distributed around the blast hole, and the crushing area of ASCB is more concentrated in the direction of energy accumulation. Therefore, ASCB can adapt to different rock strengths and achieve a better blasting effect than CSCB.

5.2 Simulation of shaped charge blasting with various decoupling coefficients

In practical projects, smooth blasting usually adopts radial uncoupled charge and axial interval charge to reduce the damage to the reserved rock mass. Usually, the damage factor is calculated to judge the uncoupled coefficient that should be adopted in the project[39]. To verify the applicability of ASCB to blasting with different decoupling coefficients, the decoupling coefficients (K_d) are changed by

changing the size of the blast-hole, and K_d=1.5, 2.0, 2.5 and 3.0 (K_d=R/r, where r is the radius of explosive; and R is the radius of blast-hole) in the range of commonly used decoupling coefficients for smooth blasting are selected[40], other parameters remain unchanged.

Results of shaped charge blasting with different decoupling coefficients are shown in Fig.16 and Fig.17. For CSCB, when K_d=1.5, through-going cracks formed in the non-energy accumulation direction, and only on the left side in the energy accumulation direction. The shape of the crushing zone is hexagonal, and the crushing zone in the energy accumulation direction is longer than that in the non-energy accumulation direction; when K_d =2.0, a penetrative crack is formed in the direction of energy accumulation, while the crack length in the non-energy accumulation direction is shorter, and the shape of the crushing zone is still hexagonal, slightly protruding in the direction of energy accumulation; when K_d =2.5, through-going cracks are formed in the non-energy accumulation direction, and only on the left side in the energy accumulation direction, and shape of the crushing zone is roughly circular; when K_d =3.0, a through-going crack is only formed on the right side in the direction of energy accumulation, and only below in the direction of non-energy accumulation. The shape of the crushing zone is circular. For ASCB, penetrating cracks are formed in the horizontal direction under four working conditions of K_d =1.5, K_d =2.0, K_d =2.5, and K_d =3.0. When K_d =3.0, penetrating cracks are also formed in the non-energy accumulation direction, and the shape of the crushing zone in all cases is gyroscopic. The crushing zone generated in the energy accumulation direction is longer than that in the non-energy accumulation direction. As the decoupling coefficient increases, the energy accumulation effect exhibited in the crushing zone gradually decreases.

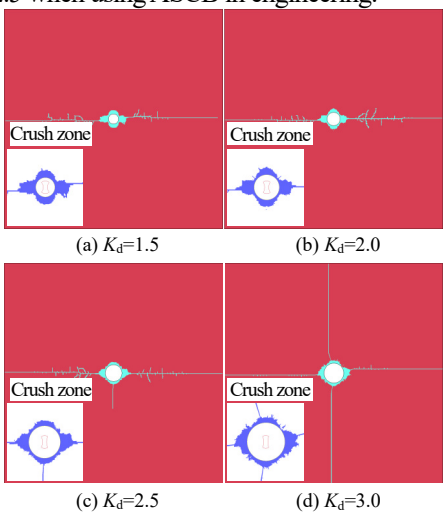


(a) K_d=1.5 (b) K_d=2.0

(c) K_d=2.5 (d) K_d=3.0

Fig.16 Results of CSCB under different decoupling coefficients

According to the above results, CSCB can only achieve good results when K_d=2.0, but the damage to the reserved rock mass is still greater than ASCB; when K_d =1.5−2.5, ASCB only forms through-going cracks in the concentrated energy direction, and almost no secondary cracks are formed in the non-concentrated energy direction. Therefore, it is recommended to adopt a decoupling coefficient range of 1.5−2.5 when using ASCB in engineering.



(a) K_d=1.5 (b) K_d=2.0

(c) K_d=2.5 (d) K_d=3.0

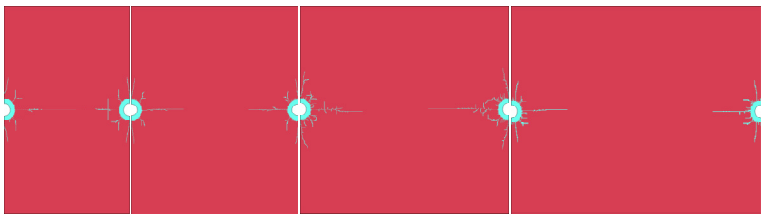
Fig.17 Results of ASCB under different decoupling coefficients

5.3 Numerical simulation of double hole blasting

The through-going cracks between smooth blasting blast-holes are the result of the joint action of adjacent blast-holes. After the blasting of adjacent blast-holes, the stress superposition will occur between blast-holes, which will promote the cracks between blast-holes to expand along the direction of the blast-hole line until they penetrate[41]. Therefore, to explore whether ASCB plays a positive role in the formation of through-going cracks between adjacent blast-holes, a double-hole blasting model was established and a CSCB was established for comparison. To reduce the amount of calculation, half holes with hole spacing L of 60 cm, 80 cm, 100 cm, and 120 cm were established, and the model heights were all 1 m. CSCB was only different from ASCB in charge shape, and the other parameters were consistent. The results of rock mass damage caused by CSCB and ASCB with different blast-hole spacings are shown in Fig.18 and Fig.19.

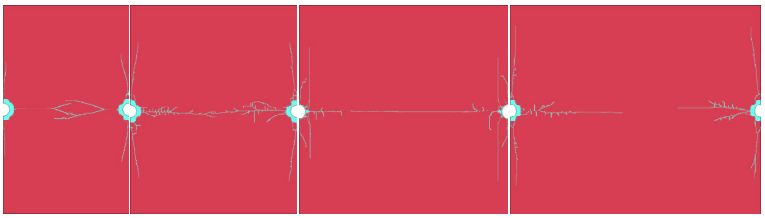
By comparing the results of single-hole ASCB (Fig.15(a)) and double-hole ASCB (Fig.19(b)), it can be found that nonthrough-going cracks are formed in the single hole, but through-going cracks have been formed in double-hole blasting with a hole spacing of 100 cm, which shows that the existence of adjacent holes has a positive effect on the formation of through-going cracks between holes. When L=60 cm, both CSCB and ASCB have formed through-going cracks, the through-going cracks generated by ASCB are not straight lines, but bifurcate in the middle, causing relatively large damage to the retained rock mass. To explore the cause of this phenomenon, the stress wave propagation process of double hole ASCB with L=60 cm is extracted, as shown in Fig.20. At t=96 μs, the stress superposition appears in the middle of the

blast-hole, and the cracks appear bifurcation at the same time due to the large tensile stress. At t=96 μs to t=164 μs, the crack continues to extend to the middle. At t=180 μs, the tensile stress zone starts to overlap, and the cracks on the left also appear bifurcation at this time. At t=212 μs, the crack continues to extend along the direction of splitting until the tensile stress is less than the compressive strength. It can be found that stress superposition is the main factor leading to fracture bifurcation. With the increase of blast-hole spacing, the strength after the stress superposition decreases, and the bifurcation will no longer occur. The CSCB cannot form through-going cracks between blast-holes at L=80 cm, L=100 cm and L=120 cm. When L=80 cm and L=100 cm, ASCB can still form through-going cracks between blast-holes, and the cracks are straight, so the effect of forming cracks is good. When L=120 cm, ASCB can no longer form through hole cracks.



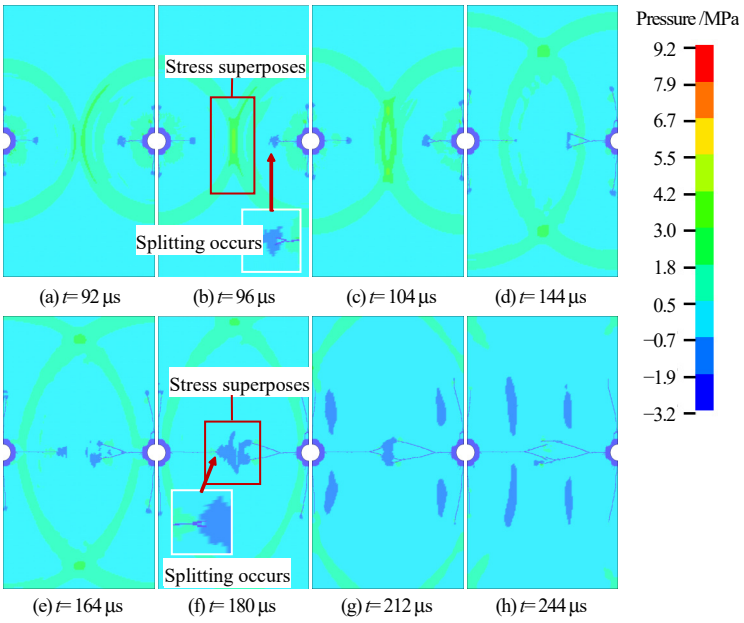
(a) L= 60 cm (b) L= 80 cm (c) L= 100 cm (d) L= 120 cm

Fig.18 Results of rock mass damage caused by double-hole CSCB with different blast-hole spacings



(a) L= 60 cm (b) L= 80 cm (c) L= 100 cm (d) L= 120 cm

Fig.19 Results of rock mass damage caused by double-hole ASCB with different blast-hole spacings



(a) t= 92 μs (b) t= 96 μs (c) t= 104 μs (d) t= 144 μs

(e) t= 164 μs (f) t= 180 μs (g) t= 212 μs (h) t= 244 μs

Fig.20 Stress wave propagation process of double hole ASCB when L=60cm

From the above results, it can be concluded that ASCB can still form through-going cracks between adjacent blast-holes when the blast-hole spacing is 100 cm, and its crack-forming effect is better than CSCB. Larger blast-hole spacing can reduce the drilling amount, thus improving the construction efficiency of the drilling blasting method.

6 Conclusion

In this study, an innovative arc-shaped charge blasting (ASCB) technique is proposed, and its performance is compared with that of the conventional cone-shaped charge blasting (CSCB) through numerical simulation. The following main conclusions are drawn:

(1) ASCB utilizes a PVC pipe as an energy-gathering device, which is cost-effective and convenient for widespread application. It requires 43.4% less explosive

than CSCB, and the efficiency of ASCB in the charge direction is 25.97% higher than that of CSCB, leading to reduced blasting vibration and improved economic benefits.

(2) Through the analysis of the formation process of initial stress waves of CSCB and ASCB, the time history curve of blast-hole wall pressure, and the propagation law of rock fractures, the results show that ASCB is more conducive to the formation of initial fractures, and the energy is more concentrated in the direction of energy accumulation, while the stress level in the direction of non-energy accumulation is lower than that of CSCB, and the directional fractures formed are about twice as large as that of CSCB.

(3) The ASCB under different rock strengths and different decoupling coefficients is studied, and the double hole blasting model with the spacing of 60 cm, 80 cm, 100 cm and 120 cm is established. The calculation results show that ASCB can be applied to various decoupling coefficient conditions, and the crack formation effect is best when the decoupling coefficient is 1.5−2.5; The higher the rock strength is, the fewer small cracks are formed, and the length of directional cracks is reduced. Under the condition of 1.0 m blast-hole spacing, ASCB can still form through-going cracks between blast-holes, which is better than that of CSCB.

The introduction of the arc-shaped charge structure presents a novel methodology for blasting applications in hydraulic engineering, tunnel excavation in transportation projects, and mining practices. This innovative approach is poised to enhance the efficiency of explosive usage and management, potentially leading to significant advancements in these fields.

Conflicts of Interest

The authors declared that they have no conflicts of interest to this work.

References

[1] HE Man-chao, CAO Wu-fu, SHAN Ren-liang, et al. New technology for two-way polygonal tensile blasting[J]. **Chinese Journal of Rock Mechanics and Engineering**, 2003, 22(12): 2047−2051.

[2] MA G W, AN X M. Numerical simulation of blasting-induced rock fractures[J]. **International Journal of Rock Mechanics and Mining Sciences**, 2008, 45(6): 966−975.

[3] YANG X J, LIU C K, JI Y G, et al. Research on roof cutting and pressure releasing technology of directional fracture blasting in dynamic pressure roadway[J]. **Geotechnical and Geological Engineering**, 2019, 37: 1555−1567.

[4] QIU P, YUE Z W, JU Y, et al. Characterizing dynamic crack-tip stress distribution and evolution under blast gases and reflected stress waves by caustics method[J]. **Theoretical and Applied Fracture Mechanics**, 2020, 108: 102632.

[5] WANG Y B. Study of the dynamic fracture effect using slotted cartridge decoupling charge blasting[J]. **International Journal of Rock Mechanics and Mining Sciences**, 2017, 96: 34−46.

[6] YANG L Y, HUANG C, BAO S J, et al. Model experimental study on controlled blasting of slit charge in deep rock mass[J]. **Soil Dynamics and Earthquake Engineering**, 2020, 138: 106318.

[7] LI Q, GAO Z H, XU W L, et al. Experimental research on the dynamic propagation process of mode I cracks in the rock under directional fracture blasting using the strain gauge method[J]. **Engineering Fracture Mechanics**, 2020, 235: 107113.

[8] HU J Z, ZHANG X Y, GAO Y B, et al. Directional presplit blasting in an innovative no-pillar mining approach[J]. **Journal of Geophysics and Engineering**, 2019, 16: 875−893.

[9] ZHANG Q, WANG J, GUO S, et al. Shaped charge hydraulic blasting: an environmental, safe, and economical method of directional roof cutting[J]. **Geofluids**, 2021, 2021: 5511081.

[10] AGU H O, HAMEED A, APPLEBY-THOMAS G J. Application of shell jetting analysis to determine the location of the virtual origin in shaped charges[J]. **International Journal of Impact Engineering**, 2018, 122: 175−181.

[11] LUO Y, SHEN Z W. Study on orientation fracture blasting with shaped charge in rock[J]. **Journal of University of Science and Technology Beijing, Mineral, Metallurgy, Material**, 2006, 13(3): 193−198.

[12] MEJÍA N, MEJÍA R, TOULKERIDIS T. Characterization of blast wave parameters in the detonation locus and near field for shaped charges[J]. **Mathematics**, 2022, 10(18): 3261.

[13] SONG Y Q, LI X S, GUO D Y, et al. Study on the decoupled charge effect in deep-hole cumulative blasting of coal seam[J]. **Advances in Civil Engineering**, 2019, 2019: 8486198.

[14] SVIRSKY O V, VLASOVA M A. On the penetration capability of shaped charges with conical and hemispherical liners[J]. **Combustion Explosion and Shock Waves**, 2019, 55: 739−743.

[15] WU B, XU S X, MENG G W, et al. Study on the dynamic evolution of through-crack in the double hole of elliptical bipolar linear-shaped charge blasting[J]. **Shock and Vibration**, 2021, 2021: 3792765.

[16] PAN Y B, ZHENG M L, XING Z Q. Experimental study on the effect of charge structure of blasting on damage to dirt band in thin coal seam[C]//IOP Conference Series: Earth and Environmental Science. [S. l.]: IOP Publishing Ltd., 2019: 022138.

[17] WANG Q B, ZHANG X, GONG B, et al. Study and application of rock breaking mechanism of concentrated water hydraulic smooth blasting in broken sand-stone geological conditions[J]. **Shock and Vibration**, 2022, 2022: 4999800.

[18] WU B, WEI H, XU S X, et al. Analysis of the cracking mechanism of an elliptical bipolar linear-shaped charge

blasting[J]. **Advances in Civil Engineering**, 2021, 2021: 6669704.

[19] LIU D W, ZHANG J J, TANG Y, et al. Damage analysis of concrete structure under multidirectional shaped charge blasting using model experiment and ultrasonic testing[J]. **Advances in Civil Engineering**, 2021, 2021: 6677041.

[20] GUO P F, YE K K, TAO Z G, et al. Experimental study on key parameters of bidirectional cumulative tensile blasting with coal-containing composite roof[J]. **KSCE Journal of Civil Engineering**, 2021, 25(5): 1718−1731.

[21] YANG J H, LU W B, HU Y G, et al. Numerical simulation of rock mass damage evolution during deep-buried tunnel excavation by drill and blast[J]. **Rock Mechanics and Rock Engineering**, 2015, 48(5): 2045−2059.

[22] ZHANG X Y, HU J Z, XUE H J, et al. Innovative approach based on roof cutting by energy-gathering blasting for protecting roadways in coal mines[J]. **Tunnelling and Underground Space Technology**, 2020, 99: 103387.

[23] LI Bi-hong. Research on theory and application technology of elliptic bipolar linear shaped charge's presplit blasting[D]. Changsha: Central South University, 2013.

[24] REIFARTH C, CASTEDO R, SANTOS A P, et al. Numerical and experimental study of externally reinforced RC slabs using FRPs subjected to close-in blast loads[J]. **International Journal of Impact Engineering**, 2021, 156: 103939.

[25] AKSHAYA GOMATHI K, RAJAGOPAL A, SURIYA PRAKASH S. Predicting the failure mechanism of RC slabs under combined blast and impact loading[J]. **Theoretical and Applied Fracture Mechanics**, 2022, 119: 103357.

[26] KUCEWICZ M, BARANOWSKI P, MAŁACHOWSKI J. Dolomite fracture modeling using the Johnson-Holmquist concrete material model: parameter determination and validation[J]. **Journal of Rock Mechanics and Geotechnical Engineering**, 2021, 13(2): 335−350.

[27] BARANOWSKI P, KUCEWICZ M, PYTLIK M, et al. Shock-induced fracture of dolomite rock in small-scale blast tests[J]. **Journal of Rock Mechanics and Geotechnical Engineering**, 2022, 14(6): 1823−835.

[28] LINFORTH S, TRAN P, RUPASINGHE M, et al. Unsaturated soil blast: flying plate experiment and numerical investigations[J]. **International Journal of Impact Engineering**, 2019, 125: 212−228.

[29] DO T V, PHAM T M, HAO H. Stress wave propagation and structural response of precast concrete segmental columns under simulated blast loads[J]. **International Journal of Impact Engineering**, 2020, 143: 103595.

[30] FENG Jia-qiang. Study on dynamic response of surrounding rock with energy-gathering smooth hydraulic blasting[D]. Wuhan: Huazhong University of Science and Technology, 2019.

[31] LI Hong-tao, WANG Zhi-qiang, YAO Qiang, et al. Study of dynamic characteristics and blasting crack propagation of quartz mica schist[J]. **Chinese Journal of Rock Mechanics and Engineering**, 2015, 34(10): 2125−2141.

[32] LV J L, ZHENG B B, LIU Z, et al. Controlled shaped-charge blasting technology for deep underground tunnel engineering[J]. **Gradevinar**, 2023, 75(10): 997−1011.

[33] MENG N K, CHEN Y, BAI J B, et al. Numerical simulation of directional fracturing by shaped charge blasting[J]. **Energy Science & Engineering**, 2020, 8(5): 1824−1839.

[34] LI M, ZHU M, LIU R F, et al. Study of the effect of empty holes on propagating cracks under blasting loads[J]. **International Journal of Rock Mechanics and Mining Sciences**, 2018, 103: 186−194.

[35] JEONG H, JEON B, CHOI S, et al. Fracturing behavior around a blasthole in a brittle material under blasting loading[J]. **International Journal of Impact Engineering**, 2020, 140: 103562.

[36] YIN Y, SUN Q, ZOU B P, et al. Numerical study on an innovative shaped charge approach of rock blasting and the timing sequence effect in microsecond magnitude[J]. **Rock Mechanics and Rock Engineering**, 2021, 54(9): 4523−4542.

[37] Ministry of Housing and Urban Rural Development of the People's Republic of China. GB 50487−2008 Code for engineering geological investigation of water resources and hydropower[S]. Beijing: China Planning Press, 2008.

[38] CAI Mei-feng. Rock mechanics and engineering[M]. Beijing: Science Press, 2013.

[39] PAN Q, ZHANG J C, ZHENG S Y, et al. Theoretical study on radial distribution laws of rock mass damage factors under decoupled charge blasting[J]. **Shock and Vibration**, 2020, 2020: 6971702.

[40] LIANG Wei-min, LIU Hong-yuan, ZHOU Feng-jun. Effect of uncoupled charge structure on rock blasting[J]. **Transactions of Beijing Institute of Technology**, 2012, 32(12): 1215−1218, 1228.

[41] HUANG Tao, CHEN Peng-wan, ZHANG Guo-xin, et al. Simulation of rock double-hole blasting process by the streamwise element method[J]. **Explosion and Shock Waves**, 2006, 26(5): 434−440.